Conformational H-bonding Modulations of the Iron Active Site Cysteine Ligand of Superoxide Reductase: Absorption and Resonance Raman Studies

Alain Desbois, Julien Valton, Yohann Moreau, Stéphane Torelli, Vincent Nivière

ARTICLE

Conformational H-bonding Modulations of the Iron Active Site Cysteine Ligand of Superoxide Reductase: Absorption and Resonance Raman Studies†

Received 00th January 20xx,
Accepted 00th January 20xx

DOI: 10.1039/x0xx00000x

Alain Desbois,[a] Julien Valton,‡[b] Yohann Moreau,[b] Stéphane Torelli,[b] and Vincent Nivière*[b]

Superoxide reductases (SORs) are mononuclear nonheme iron enzymes involved in superoxide radical detoxification in some microorganisms. Their atypical active site is made of an iron atom pentacoordinated by four equatorial nitrogen atoms from histidine residues and one axial sulfur atom from a cysteinate residue, which plays a central role in catalysis. In most SORs, the residue immediately following the cysteinate ligand is an asparagine, which belongs to the second coordination sphere and is expected to have a critical influence on the properties of the active site. In this work, in order to investigate the role of this asparagine residue in the *Desulfoarculus baarsii* enzyme (Asn117), we carried out, in comparison with the wild-type enzyme, absorption and resonance Raman (RR) studies on a SOR mutant in which Asn117 was changed into an alanine. A RR analysis was developed in order to assign the different bands using an excitation in the (Cys116)-$S^- \rightarrow Fe^{3+}$ charge transfer band. By investigating the correlation between the (Cys116)-$S^- \rightarrow Fe^{3+}$ charge transfer band maximum with the frequency of each RR band in different SOR forms, we assessed the contribution of the ν(Fe-S) vibration among the different RR bands. The data showed that Asn117, by making hydrogen bond interactions with Lys74 and Tyr76, allows a rigidification of the backbone of the Cys116 ligand, as well as that of the neighboring residues Ile118 and His119. Such a structural role of Asn117 has a deep impact on the S-Fe bond. It results in a tight control of the H-bond distance between the Ile118 and His119 NH peptidic moiety with the cysteine sulfur ligand, which in turn enables a fine tuning of the S-Fe bond strength, an essentiel property for the SOR active site. This study illustrates the intricate roles of second coordination sphere residues to adjust the ligand to metal bond properties in the active site of metalloenzymes.

1. Introduction

Oxidative stress is a major problem encountered by living organisms. It originates from an abnormal formation of reactive oxygen species in cells, resulting from a cascade of one electron reduction of molecular dioxygen (O_2) into superoxide radical ($O_2^{\bullet-}$) as the first appearing toxic species.[1,2] Whereas superoxide dismutases (SOD) have been described for long to be involved in $O_2^{\bullet-}$ detoxification, and thus protection against oxidative stress, superoxide reductases (SORs) appeared more recently as an alternative $O_2^{\bullet-}$ eliminating system in some anaerobic or microaerophilic microorganisms. Such microorganisms encounter oxidative stress conditions, at least transiently, and SORs play an important role for their survival to O_2 exposure.[3]

SORs are iron-containing enzymes that catalyze the one electron reduction of $O_2^{\bullet-}$ into H_2O_2 (Eq.1), without production of O_2.[4–9] The electrons involved in this reaction are provided by cellular reductases, as physiological SORs partners :[10,11]

$$O_2^{\bullet-} + 1e^- + 2H^+ \rightarrow H_2O_2 \quad \text{(Eq. 1)}$$

The active site of SORs consists in an atypical nonheme mononuclear ferrous iron center, pentacoordinated in a square pyramidal geometry by four equatorial nitrogen atoms from histidines and one axial sulfur atom from a cysteine ([FeN_4S_1]).[12–18] Whereas this active site is common to all SORs described so far, seven different classes of SORs were proposed based on sequence alignments and the presence of additional structural domains.[19] Nevertheless, only classes I, II and III have been extensively characterized so far.[9] Class I SORs, or 2Fe-SORs present in *Desulfoarculus baarsii* (*Db*)[5,14,15] and *Desulfovibrio vulgaris* (*Dv*)[6] enzymes are homodimeric and contain a second mononuclear iron center located in an additional N-terminal domain. This center is of desulforedoxin type (Dx), with a ferric iron chelated by four sulfur atoms from cysteines ([FeS_4]) in a rubredoxin-distorted manner.[20] It is located 22 Å away from the active site and its function in catalysis is not clearly established yet.[21–23] Class II SORs, like in *Pyrococcus*

[a] *Institute for Integrative Biology of the Cell (I2BC), CEA, CNRS, Univ Paris-Sud, Université Paris-Saclay, F-91198, Gif-sur-Yvette Cedex, France.*
[b] *Univ. Grenoble Alpes, CNRS, CEA, IRIG-LCBM, F-38000 Grenoble, France. E-mail: vniviere@cea.fr; Tel: (33) 4 38 78 91 09.*
† Electronic Supplementary Information (ESI) available: Figs. S1, S2, S3, S4 and S5; Tables S1 and S2. See DOI: 10.1039/x0xx00000x
‡ Present address: Cellectis, 8 rue de la Croix Jarry, 75013 Paris, France.

furiosus (*Pf*), do not have the Dx N-terminal domain and are homotetrameric enzymes.[13] They contain only the iron active site center and are thus called 1Fe-SORs. Finally Class III SORs, like in *Treponema pallidum* (*Tp*),[16] contain the additional N-terminal domain but with only one of the four cysteine ligands and therefore lacks the Dx iron center. Like Class I, Class III SORs are homodimeric enzymes and their overall X-ray structures are very similar.

The catalytic cycle of SORs has been extensively studied, both experimentally[24–27] and theoretically.[28–30] All the data agree with an inner sphere reduction mechanism, involving $O_2^{\bullet-}$ binding at the free sixth coordination position of the ferrous center as first step. This reaction is extremely fast and together with a single protonation process, the reduction of $O_2^{\bullet-}$ leads to the formation of a high-spin ferric iron hydroperoxide intermediate (Fe^{3+}-OOH). In the case of *Db* SOR, this intermediate has been trapped and characterized by high-resolution X-ray structure,[15] resonance Raman[31,32] and Mössbauer[33] spectroscopies.

A second step, consisting in the specific protonation on the proximal oxygen of the hydroperoxide moiety, has been proposed to lead to the formation of H_2O_2. X-ray structures of the Fe^{3+}-OOH intermediate suggest that Lys48 (numbered accordingly to *Db* SOR sequence), a highly conserved residue located close to the iron site, could play a pivotal role in this step.[15] Accordingly, it was shown that mutation of Lys48 into an isoleucine (K48I mutant) in the *Db* SOR modifies the fate of the Fe^{3+}-OOH intermediate and favors the formation of a high valent iron-oxo species (Fe^{IV}=O), through a O-O bond cleavage.[34] The formation of such an iron-oxo species in the K48I mutant was associated with the lack of a specific protonation process at the proximal oxygen of the Fe^{3+}-OOH intermediate, most-likely favoring a double protonation of its distal oxygen and subsequent O-O bond cleavage, as it naturally occurs in cytochrome P450 oxygenase for substrates oxidation.[35] Thus, the mechanisms by which SORs control the protonation and the evolution of the Fe^{3+}-OOH intermediate appears to be determinant for its activity. Finally, H_2O_2 release is followed by the monodentate coordination of a carboxylate side chain of a highly-conserved glutamate residue (Glu47 in *Db*), which then becomes the sixth ligand of the high-spin ferric site.[13,36,37]

Lys48 is not the only neighboring residue that helps tuning the reactivity of the SORs active site. X-ray data suggest that Ile118 and His119 (numbering according to *Db* sequence) make H-bond interactions through their NH main chains with the sulfur atom of the cysteinate ligand (Cys116) (Fig. 1). Site-directed mutagenesis experiments on Ile118 associated with DFT calculations showed that this H-bond network modulates the electron-donor properties of the thiolate of the Cys ligand to the iron, allowing a control of the p*Ka* of the first reaction intermediate and its protonation rate.[38]

Interestingly, the X-ray structures of SORs also indicate that the side chain of the Asn117 (*Db* numbering) is the closest to the sulfur atom of the Cys ligand (Fig. 1).[12–18] Asn117 is highly conserved among SORs sequences and belongs to the Cys116-Asn117-Ile118-His119 tetrapeptide that forms a bidentate chelate, *via* S(Cys116) and N(His119), to the iron active site. These data suggest that Asn117 might be as well involved in the control of the S-Fe bond strength.

In this work, in order to investigate the potential role of Asn117 toward the properties of the active site, a resonance Raman (RR) study on a N117A mutant was carried out using an excitation in the $(Cys)S^- \rightarrow Fe^{3+}$ charge transfer (CT) band. The active modes, thus enhanced, predominantly arise from the Fe^{3+}-S(Cys) moiety. In SORs, previous RR studies provided valuable information on the S-Fe strength and cysteine ligand conformations.[39,40] They also appeared well adapted to characterize effects of mutations of second coordination sphere residues on the iron active site, which may not be deduced from X-ray structures.[38,41] Here, we show that Asn117 allows a rigidification of the Cys116-Asn117-Ile118-His119 tetrapeptide. This results in a tight control of the H-bond distance between the Ile118 and/or His119 NH peptide and the Cys sulfur ligand, which, as underlined above, allows a fine tuning of the S-Fe bond properties.

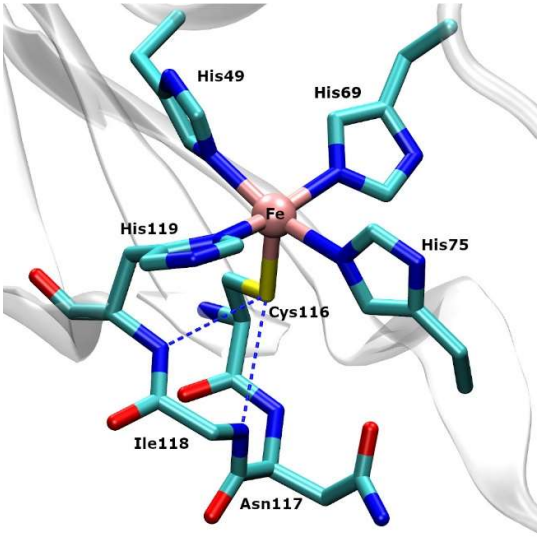

Fig. 1. Scheme of the ferrous iron active site of the wild-type SOR from *D. baarsii* from its crystal structure,[15] together with the Cys116-Asn117-Ile118-His119 tetrapeptide chelate. Hydrogen bonds are shown as dotted blue lines between the amide NH main chains of Ile118 (2.4 Å) and His119 (2.2 Å) and the S atom of the Cys116 ligand. The side chain of Ile118 is not shown for clarity. The distances between S(Cys116) and the O and N atoms of the side chain of Asn117 are 4.1 Å and 6.1 Å respectively.

2. Experimental procedures

Site-directed mutagenesis and protein purification

Mutagenesis was carried out on the plasmid pMJ25,[5] with the QuickChange® site-directed mutagenesis kit from Stratagene. Plasmid pMJ25 is a pJF119EH derivative in which the *sor* gene from *Desulfoarculus baarsii* was cloned under the control of a *tac* IPTG inducible promotor. Two primers were designed for the PCR-based site-directed mutagenesis to create the N117A SOR mutant, primer 1 (5' GCC CGC GAA TAC TGC GCG ATC CAC GGC CAC TGG 3') and primer 2 (5' CCA GTG GCC GTG GAT CGC GCA GTA TTC GCG GGC 3'). The mutation was verified by DNA sequencing. The resulting plasmid, pMJ25 N117A, was transformed into an *E. coli* BL21 strain. Over-expressions and purifications of the wild-type and N117A mutant proteins were carried out as reported previously.[27] The purified mutant protein appeared to be homogeneous as judged by SDS-PAGE analysis. Protein concentrations were determined using the Bio-Rad® protein assay reagent. For the SOR mutant, full metalation of the two mononuclear iron sites was verified by atomic absorption spectroscopy. The N117A SOR mutant was isolated with an oxidized Dx center (ε_{503nm} = 4,400 M^{-1} cm^{-1}) and a reduced active site. Fully oxidized SOR, with its active site in a ferric state, was obtained by treatment with a slight molar excess of K_2IrCl_6.

pH studies

The following buffers were used to cover a pH range from 5.75 to 9.85: MES for pHs 5.75, 6.10 and 6.60; Bis-Tris propane or HEPES for pH 6.80; Tris-HCl for pHs 7.60, 8.00, 8.50 and 8.90; glycine-NaOH for pHs 9.15, 9.40 and 9.85. The apparent pK_a of the SOR alkaline transition was determined from the pH dependence of the absorbance at 645 nm of the fully oxidized protein.[24] The titration curve was fitted with an equation expected for a single protonation process: $A_{645nm} = (A_{645max} + A_{645min} \times 10^{(pH-pKa\ app)})/(1 + 10^{(pH-pKa\ app)})$.

Electronic absorption and EPR spectroscopies

Optical absorbance measurements were performed using a Varian Cary spectrophotometer (0.2 nm bandwidth) with 1 cm path length cuvettes. Low-temperature (7 K) X-band EPR spectra were recorded on a Bruker EMX spectrometer equipped with an Oxford Instrument ESR 910 cryostat. The microwave frequency was calibrated with a frequency counter and the magnetic field with a NMR gaussmeter.

Resonance Raman spectroscopy

For the resonance Raman (RR) experiments, 3.5 µl of the concentrated protein (4-6 mM) were deposited onto a glass slide sample holder and then transferred into a cold helium gas circulating optical cryostat (STVP-100, Janis Research), held at 15 K. RR spectra were recorded using a Jobin-Yvon U1000 spectrometer, equipped with a liquid nitrogen-cooled CCD detector (Spectrum One, Jobin-Yvon, France). The 647.1 nm-excitation (30 mW) was provided by an Innova Kr^+ laser (Coherent, Palo Alto). Signal-to-noise ratios were improved by spectral collections of 6 cycles of 30 s accumulation time. The spectrometer calibration was done as previously described.[42] The frequencies of the RR bands were internally calibrated against the main band of the ice lattice (230 cm^{-1}). The RR contribution of the SOR Dx center was subtracted using its specific bands at 309, 347, 382, 623 and 692 cm^{-1}.[32] In the 200-320 cm^{-1} region, Raman signals of the ice were also removed. All these spectral treatments, as well as the spectral analysis, were made using the Grams 32 software (Galactic Industries). The frequency precision was 0.5-1 cm^{-1} for the most intense bands and 1.5-2 cm^{-1} for the weakest ones.

3. Results

Electronic absorption and EPR spectroscopies of the *D. baarsii* (*Db*) SOR N117A mutant

The UV-visible absorption spectrum of the as-isolated N117A mutant exhibits the characteristic bands at 370 nm and 503 nm arising from the rubredoxin-like Dx ferric iron center (data not shown).[5] When treated with K_2IrCl_6, the spectrum shows an increase of absorbance in the 500-700 nm region, in agreement with the oxidation of the iron active site and associated with a $(Cys)S^- \rightarrow Fe^{3+}$ CT transition (Fig. 2A).[36,40]

The 7 K EPR spectrum of the N117A mutant displays resonances at g = 7.7, 5.7, 4.1 and 1.8, identical to those obtained for the WT protein and originating from the Dx center.[5] The EPR spectrum of the K_2IrCl_6-oxidized N117A mutant exhibits an additional signal at g = 4.3, similar to that observed for the WT SOR (Fig. 2B) [5] and assigned to a rhombic (E/D = 0.33) high-spin (S = 5/2) ferric ion center.[40] On note, the spectrum of the oxidized active site of the mutant displays a more pronounced splitting of the low-field component compared to that observed for the WT (Fig. 2B). This could reflect subtle changes in the g-tensor rhombicity in the mutant. Nevertheless, these data showed that the N117A mutation does not disturb the overall structure of the *Db* SOR.

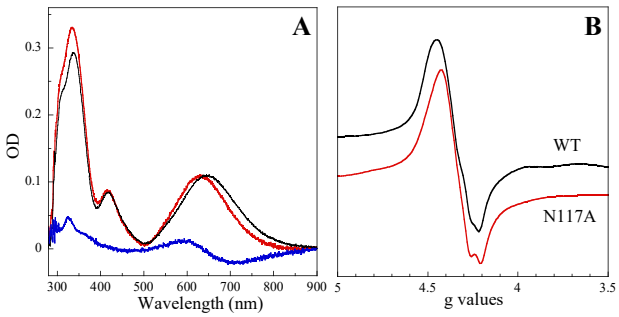

Fig. 2. (A) Electronic absorption spectra of the oxidized active site of the *D. baarsii* SOR, WT (black) and N117A mutant (red). Proteins (60 µM) were in 50 mM HEPES buffer, pH 7.5. The traces result from spectral differences of the fully K_2IrCl_6-oxidized minus the as-prepared SORs. The difference spectrum between N117A mutant and WT SOR is shown in blue. (B) X-band EPR spectra of the oxidized active site of the WT (black) and N117A mutant (red) SORs from *D. baarsii*. The proteins (150 µM) were in 50 mM HEPES buffer, pH 7.5. The signals result from spectral differences between fully K_2IrCl_6-oxidized and as-prepared SORs. Experimental conditions: temperature 7 K, microwave power 1 mW at 9.42 GHz, modulation amplitude 1 mT at 100 kHz.

As reported for the WT *Db* SOR,[24] the absorption band maximum of the ferric iron active site of the N117A mutant was blue-shifted at alkaline pHs (Fig. S1). This process reflects the displacement of its sixth coordinating ligand (carboxylate side chain of Glu47) by a hydroxide ion.[43] The associated apparent pK_a for the N117A mutant was found to be 8.65 ± 0.05 (Fig. S1), a value slightly lower than that reported for the WT protein (9.00 ± 0.10).[24] Interestingly, the absorbance band maximum of the Fe^{3+}-Glu47 form of the N117A mutant (acidic to neutral pHs) was found at 625 nm (ε = 1.9 mM^{-1} cm^{-1}), a value blue-shifted by -19 nm compared to that reported for WT SOR (644 nm, Fig. 2A).[24] Moreover, the CT band half-height width decreased by 13 nm in the mutant spectrum (140 *vs* 153 nm in the WT) (Fig. 2A).

Since these bands correspond to a CT transition of $\pi \rightarrow \pi^*$ character ($(Cys)S(p\pi) \rightarrow Fe^{3+}(d\pi_{p\ xy})$),[36] an increased transition energy as observed in the N117A mutant strongly suggests a less favorable $(Cys)S^- \rightarrow Fe^{3+}$ electron transfer. This could result from an increase of the H-bonding interactions towards the S(Cys) ligand (Fig. 1), which by relocalizing the π-electron density of the S-Fe bond toward the S atom makes the $S^- \rightarrow Fe^{3+}$ CT transition higher in energy. Spectral changes are also seen in the high-energy region (300-400 nm, Fig. 2A), but their interpretation is not unambiguous due to overlapping contributions of the $\sigma \rightarrow \sigma^*$ $(Cys)S^- \rightarrow Fe^{3+}$ CT with the strong π His $\rightarrow Fe^{3+}$ CTs.[36]

Resonance Raman spectroscopy of the WT and N117A *Db* SORs

Previous resonance Raman (RR) studies of the ferric SOR active site, obtained with an excitation in the $(Cys)S^- \rightarrow Fe^{3+}$ CT transition, were proposed to be largely dominated by vibrational modes arising from the Fe^{3+}-S(Cys) moiety.[39,40] These RR studies have provided valuable information on the different classes of SOR, revealing small but

functionally important differences between their active sites. These differences could not be deduced from the X-ray diffraction studies given the resolution factors.[13,15,16] Moreover, RR studies highlighted some of the local effects of mutations concerning second coordination sphere residues on the (Cys)S-Fe^{3+} bond strength.[38,41]

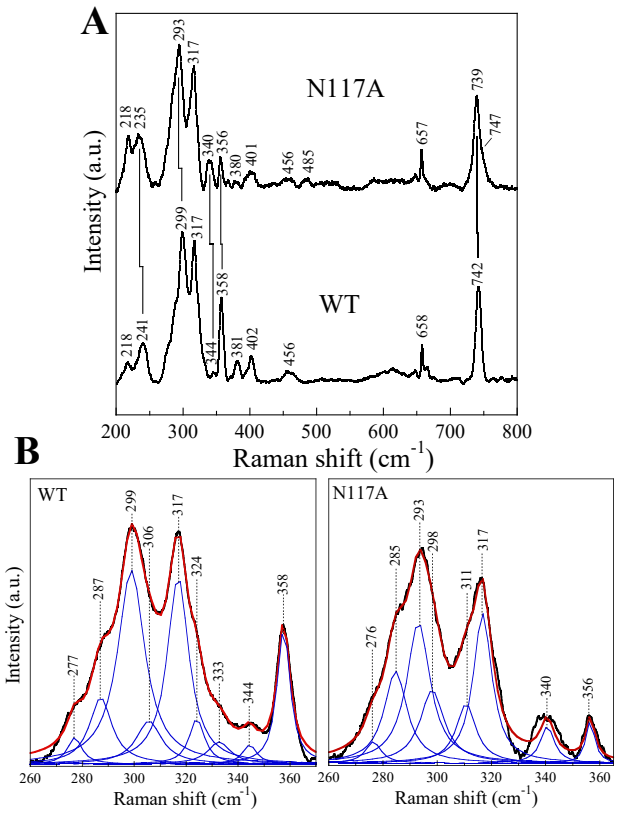

Fig. 3. (A) 200-800 cm^{-1} regions of 15 K RR spectra excited at 647.1 nm of the K_2IrCl_6-oxidized *D. baarsii* SOR, WT (lower spectrum) and N117A mutant (upper spectrum), at 6 mM in 50 mM Tris/HCl pH 7.6 buffer. For each spectrum, contributions of the Dx center and ice were subtracted. (B) Experimental and component RR spectra of the *D. baarsii* SOR WT (left) and N117A mutant (right) in the 260-370 cm^{-1} region. The RR spectra (black line) were submitted to band fitting analysis (blue and red lines) using the Spectra Calc software. Spectra were simulated as a convolution of a minimum number of Lorentzian bands with plausible bandwidths (blue), allowing the best reproduction of the experimental spectra (red).

Figure 3A shows the RR spectra of K_2IrCl_6-oxidized WT and N117A *Db* SORs using a 647.1 nm-excitation, in resonance with the $(Cys)S^- \rightarrow Fe^{3+}$ CT band. An assignment of the different RR bands of the *Db* SOR was proposed on the basis of ^{34}S- and ^{15}N- labeling RR experiments on the oxidized *Desulfovibrio vulgaris* (*Dv*) SOR,[40] which belongs to the same Class I family as the *Db* enzyme, and exhibits similar spectroscopic properties. The RR bands in the 290-510 cm^{-1} region were proposed to correspond to modes partially mixing the Fe-S stretching mode with Cys deformations and the 270-370 cm^{-1} region is expected to include the intrinsic Fe-S stretch.[39,40] By analogy with type-1 blue copper proteins,[44–46] the 299 cm^{-1} line (Fig. 3A), which is the most intense peak and exhibits the largest ^{34}S isotope sensitivity in the RR spectra of the *Dv* SOR, was pointed out to have a predominant ν(Fe-S(Cys)) character.[40]

Other ν(Fe-S(Cys))-involving modes are also expected in this low-frequency region.[39,40] In fact, the 350-510 cm^{-1} region was proposed to exhibit internal deformation modes of the coordinated Cys residue partially coupled to the Fe-S stretch ($\delta(C_\beta\text{-}C_\alpha\text{-}C(O)) + \delta(C_\beta\text{-}C_\alpha\text{-}N) + \delta(C(O)\text{-}C_\alpha\text{-}N) + \delta(C_\alpha\text{-}N\text{-}C(O)) + \delta(S\text{-}C_\beta\text{-}C_\alpha) + \nu(Fe\text{-}S)$).[40] The extents of mode mixing depend on the conformation of the Fe-S-C_β-C_α(CO)-NH-C(O) grouping, in particular on the Fe-S-C_β angle and the (Fe-S-C_β)-(S-C_β-C_α) dihedral angle.[39,40,47] On note, the axial sulfur atom is potentially involved in two peptide NH--S^- H-bonds (with NH(Ile118) and NH(His119))[38] (Fig. 1). Strong and/or well-oriented H-bonds can add coupling between modes involving the sulfur atom and the peptide amide groups. Therefore, considering the complexity of the low-frequency RR spectra, a further analysis of the *Db* SOR RR spectra was carried out in order to get detailed information regarding the specific effect of the N117A mutation in terms of bond distance and/or active site geometry.

First of all, spectral analysis of this low-frequency region is complicated due to overlapping bands. As shown in Figure 3B, for the WT and N117A *Db* SORs, band fitting analysis allows us to better characterize substantial differences in terms of number of observed bands, their frequencies, widths and relative intensities. In the case of the *Archaeglobus fulgidus* (*Af*) Class II 1Fe-SOR, the so-called "intensity weighted frequency" approach ($\langle\nu_{Fe\text{-}S}\rangle$) was used to compare the Fe-S(Cys) bond strength between WT and mutant forms.[48] This parameter is expected to represent an averaged frequency of the modes involving ν(Fe-S(Cys)), distributed among the bands of the 270-370 cm^{-1} region, and weighted by their respective intensities.[48] This approach is valid if we consider that all these RR bands contain a fractional contribution of the metal-S(Cys) stretching coordinate.[48] Such an approximation is appropriate when the intensities of the RR bands are not strongly affected.[48,49] In the case of the *Db* SOR compounds, considering the large intensity variations of a number of RR bands between the WT and mutant proteins (Fig. 2, Table S1, and reference [38]), such an analysis of the RR spectra might not be adapted to Class I SORs. Indeed, different intensity distributions among the various modes of the N117A mutant, as compared to the WT enzyme (Fig. 3A), indicate a substantial perturbation of the active site geometry.

Spectral analysis of the RR frequencies involving ν(Fe-S) modes *vs* the maximum of the SOR Fe^{3+} absorption band

In order to better identify the Fe-S(Cys) stretching contribution among the different RR bands of the WT and N117A *Db* SORs, another approach was considered. Previous works reported that the maximum of the SOR absorption band corresponding to the $(Cys)S^- \rightarrow Fe^{3+}$ CT transition depends on both the classes of SORs and on the mutations in proximity to the $Fe^{3+}(His)_4(Cys)(Glu)$ catalytic site.[32,36,38–41] This also applies in the present case for the N117A mutant, which exhibits a blue-shifted CT transition by 19 nm when compared to the WT form (Fig. 2A). Thus, among the different SORs and their mutants, the RR bands involving major contribution of ν(Fe-S) are expected to be significantly sensitive to the variations of their $(Cys)S^- \rightarrow Fe^{3+}$ CT energy.

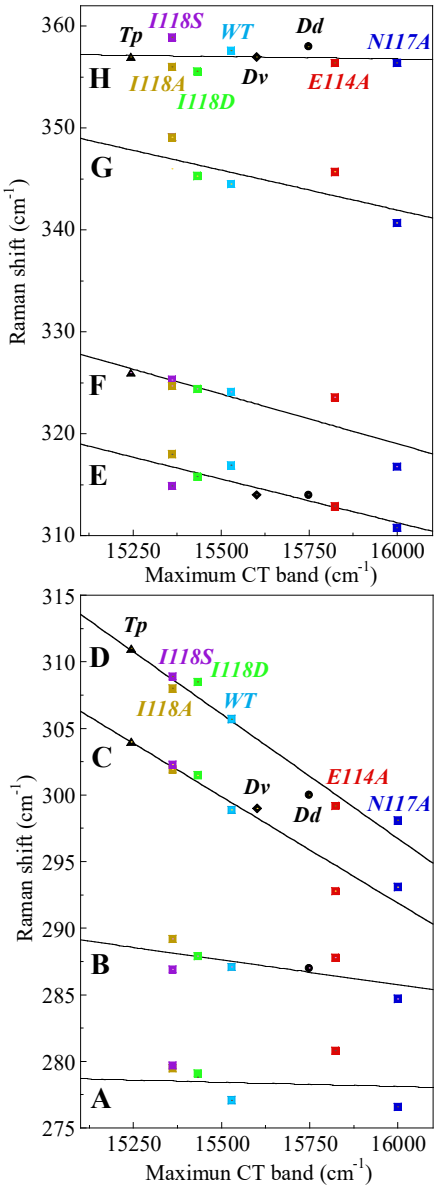

Fig. 4. Plots of the RR frequencies of ν(Fe-S)-involving modes (270-370 cm^{-1}) *vs* the maximum of the (Cys)$S^{-} \rightarrow Fe^{3+}$ CT absorption bands reported at neutral pHs for different Class I and Class III SORs, as noted on the top. *D. baarsii* SOR compounds (square), WT and mutants N117A (Table 1), I118D,[38] I118S,[38] I118A[38] and E114A[41]; Class I SORs from *Desulfovibrio vulgaris*[40] (diamond, *Dv*) and *Desulfovibrio desulfuricans*[50] (circle, *Dd*); Class III SOR from *Treponema pallidum*[32] (triangle, *Tp*). Lower plot shows RR bands A, B, C and D (Table 1). Upper plot shows RR bands E, F, G and H (Table 1). The solid lines correspond to a linear fit calculated for each set of bands (Table 1).

Resonance Raman bands of the 270-470 cm^{-1} region

Figure 4 plots the frequencies of the 270-370 cm^{-1} region RR bands reported for the Class I 2Fe-SORs from *D. baarsii* (*Db*),[32,38,41,43] *Desulfovibrio vulgaris* (*Dv*),[40] *Desulfovibrio desulfuricans* (*Dd*)[50] and for the Class III 1Fe-SOR from *Treponema pallidum* (*Tp*),[32] as a function of their CT position. On note that the frequencies of these RR and CT bands correspond to the same SOR ferric active site coordination, with the sixth coordination position occupied by the carboxylate group of the well conserved Glu47 residue, as observed under acidic to neutral pHs.[43] Interestingly, these plots show a series of linear anti-correlations with marked slopes for RR bands C, D, E, F and G (Fig. 4 and Table 1). When the absorption and RR data of the *Dv*-, *Dd*- and *Tp*- SORs are not considered, these linear anti-correlations remain mainly unaffected (data not shown). On the opposite, the spectroscopic data originating from the Class II 1Fe-SORs from *Pyrococcus furiosus*,[39] *Archaeglobus fulgidus*[48] and *Ignicoccus hospitalis*[49] do not match those of Figure 4, but rather, constitute themselves other types of linear anti-correlations (Fig. S2, Table S2). Slight but significant structural differences between the active site of SORs from Classes I and III on one side and from Class II on the other side have been reported,[39,40] which could account for the absence of correlations observed here between these classes.

As shown in Figure 4, band C (assigned to a major ν(Fe-S) mode in SOR[32,38]) exhibits one of the highest dependence on the CT absorption value, with a slope of 16.0 ± 1.5 cm^{-1} for a CT energy change of 1000 cm^{-1} (Table 1). This data supports the relevance of our analysis to identify the relative contribution of the ν(Fe-S) in the set of RR bands. In *Db* WT and mutated SORs, band C varies from 293 cm^{-1} (N117A and E114A) to 299 cm^{-1} (WT) and 302 cm^{-1} (Ile118 mutants).

Band D also exhibits a high sensitivity to the CT energy (slope = -17.9 ± 1.6 cm^{-1}/1000 cm^{-1}) and shifts in *Db* SOR from 298-299 cm^{-1} (N117A and E114A) to 306 (WT) and 308-309 cm^{-1} (I118A, I118D and I118S) (Table 1). Although band D is much less intense than band C (Fig. 3), these data suggest that it could be a good candidate for a predominant ν(Fe-S) contribution in its potential energy distribution (PED). Nevertheless, in the absence of any isotopic information,[40] a precise origin of band D is difficult to establish. It may represents an antisymmetric counterpart of the mode associated to band C. Indeed, the rhombicity of the FeN_4(His)S(Cys)O(Glu) grouping of Class I and III SORs (Fig. 2B and references[32,40]) allows for the RR activity of an antisymmetric mode involving a major Fe-S(Cys) stretch mixed with some deformations and stretching of the FeN_4(His) bonds and stretching of the trans Fe-O(Glu) bond.

Thus, in the N117A mutant, the 6-8 cm^{-1} downshifts of bands C and D, involving major ν(Fe-S) mode, indicates a markedly decrease of the strength of the S-Fe bond in this mutant.

In the 315-350 cm^{-1} region, bands E, F and G also show sensitivities to the CT position (Table 1). On the basis of ^{34}S- and ^{15}N- labeling, band E was assigned to a mode mixing S-C_β-C_α bending and Fe-S(Cys) stretching,[40] and its associated slope value of 8.8 ± 2.3 (Fig. 4 and Table 1) is consistent with such an assignment. The frequency of band E of the *Db* N117A mutant is downshifted by 6 cm^{-1} compared to the WT, again in line with a weaker S-Fe bond in this mutant. Band E intensities are also strongly decreasing in the spectra of the N117A and I118 mutants compared to the WT form. On note, an intense line was observed at 314 cm^{-1} in the spectra of the WT *Dv*- and *Dd*-SORs.[40,50] Thus, the decreased intensity of band E in the N117A mutant could be associated with noticeable changes in conformation of the Fe-S-C_β-C_α grouping.

No isotopic information is available for bands F (317-325 cm^{-1}) and G (340-349 cm^{-1}).[39,40] Nevertheless, the similarities with band E, in terms of slope values and intensity changes, suggest analogous assignments for bands F and G, namely a S-Fe bond strength decrease and a S-C_β-C_α deformations coupled to Fe-S(Cys) stretch (Table 1). Again, these data indicate that the N117A mutation affects the conformation of the Fe-S-C_β-C_α grouping.

Band H appears as an intense line at 356-359 cm^{-1} in the RR spectra of WT *Db* SOR and its E114A, I118A, I118S and I118D mutants (Fig. 3 and Table 1). For the N117A mutant, this band is detected at 356 cm^{-1}, with a marked decrease of intensity (Fig. 3). A strong line at 357 cm^{-1} for the *Dv* SOR is also sensitive to ^{15}N- and ^{34}S- labeling (- 3.4 and - 2.0 cm^{-1}, respectively).[40] Spectra of the *Dd* and *Tp* SORs show an analogous band at 358 and 357 cm^{-1}, respectively.[32,50] The frequency dispersion appears therefore limited and Fig. 4 shows that band H is unrelated to the CT energy. Thus, although mostly enhanced by the $(Cys)S^- \rightarrow Fe^{3+}$ CT transition, band H cannot be associated to a significant ν(Fe-S) stretch. It could correspond to an internal deformation of the Cys side chain (δ(S-C_β-C_α(CO)-N-C(O)), its RR activity being due to extensive coupling of the Fe-S stretch with the side chain and the peptide backbone H-bonding.[39,40] Therefore, changes in intensity of band H in the N117A mutant could reflect conformational changes of the Cys ligand induced by the mutation.

Six common bands are observed in the 370-470 cm^{-1} region of the RR spectra of the *Db* SOR derivatives (bands I-N in Table 1, Fig. S3). Only the frequency of band K (401-406 cm^{-1}) exhibits a sensitivity to the CT maximum (slope = -5.4 ± 2.0, Fig. S3, Table 1). A homologous band observed at 404 cm^{-1} for *Dv* SOR is sensitive to isotopic ^{34}S- and ^{15}N- labeling (- 1 and - 2 cm^{-1}, respectively).[40] Band K can be therefore assigned to a mode involving Fe-S stretch and S-C_β-C_α deformation mixed with major deformations of the Cys side chain.

Mid-frequency regions of the resonance Raman spectra (590-770 cm^{-1})

The 590-770 cm^{-1} region of the RR spectra of SORs is dominated by a stretching mode involving the S-C_β bond of the coordinated Cys residue (ν(SC_β)).[39,40] This band is located at 742 cm^{-1} for the WT *Db* SOR (Fig. 3).[32] In the spectra of the N117A mutant, this line is significantly downshifted to 739 cm^{-1} (Fig. 3A), supporting a decrease in strength of the S-C_β (Cys) bond. For the *Db* SOR mutants as well as for SORs from other species, it is interesting to consider that the ν(S-C_β(Cys)) frequency has a marked sensitivity to the CT energy (slope = -7.4 ± 1.6) (Fig. S4, Table 1). Therefore, the strength of the Fe-S bond also affects that of the S-C_β bond. It should be noted that shifts in ν(S-C_β(Cys)) in metalloproteins were associated with changes in (metal-S-C_β)-(S-C_β-C_α) dihedral angle.[45,47] Moreover, a variation in S-C_β(Cys)) bond strength, as observed in the N117A mutant, could be also related to a modulation in H-bonding status of the S(Cys) atom (Fig. 1). So, the decrease of the S-C_β(Cys) bond strength in the N117A mutant may be in line with an increase of the H-bonding interactions of the NH peptide positions toward the S(Cys) ligand.

Modes involving Fe-N(His) stretching (200-260 cm^{-1})

The weak bands observed in the 200-260 cm^{-1} regions of the RR spectra were assigned to either symmetric or antisymmetric Fe-N(His) stretching modes.[39,40] The spectrum of the WT *Db* SOR exhibit two bands at 218 and 241 cm^{-1} (Fig. 3A, Table 1). For the N117A mutant, we observed significant gains in intensity of the two ν(Fe-N(His)) modes and a 6 cm^{-1} downshift of the high-frequency component (241 *vs* 235 cm^{-1} in Fig. 3A). The extent of this shift is similar to that of the modes involving major ν(Fe-S(Cys)) stretch, *i.e.* bands C (- 6 cm^{-1}) and D (- 8 cm^{-1}). Therefore, spectral changes in the low-frequency region show that the N117A mutation in *Db* SOR not only affects the Fe-Cys linkage but also at least one Fe-His coordinate. The increased RR activity of the ν(Fe-N(His)) modes is likely due to an A-term mechanism, *i.e.* a distortion of the Fe-N(His) bonds in the electronic excited-state associated to the $S^- \rightarrow Fe^{3+}$ transition.[39,40] The RR spectra of *Pf*- and *Dd*- SORs show homologous bands at 210 and 241-242 cm^{-1},[39,50] and the different sensitivities of these bands to ^{54}Fe-labeling support that the 210 and 241 cm^{-1} lines correspond to symmetric and antisymmetric motions, respectively.[39] For the *Db* SORs, the sensitivities of the RR frequencies to the $(Cys)S^- \rightarrow Fe^{3+}$ CT position differ for these two ν(Fe-N(His))-involving modes (Table 1, Fig. S5). The 214-218 cm^{-1} bands do not exhibit a clear sensitivity to the CT energy (Fig. S5, Table1), whereas the slopes of the 235-241 cm^{-1} lines are relatively high (slope = -6.8 ± 2.5, Fig. S5, Table 1). This suggests that the normal mode corresponding to the 235-241 cm^{-1} band includes a stretching of the Fe-S bond and a deformation of the FeN_4(His)S(Cys)O(Glu) grouping in addition to an antisymmetric stretch of the Fe-N(His) bonds.

These RR spectral changes in the N117A mutant could therefore be associated with a significant modification of the geometry of the Fe-N_4(His)S(Cys)O(Glu) site, in line with the slight changes in the EPR spectrum (Fig. 2B).

Different factors could account for the frequency shift of the major ν_{as}(Fe-N(His)) and some geometry changes. A slight rotation of imidazole ring(s) of His ligand(s) in the N117A mutant could be proposed. Indeed, whereas the σ interaction between metal and imidazole ligand is independent of the ring position, a ring rotation around the Fe-N bond of a given His ligand is expected to modify its Fe(π) → Imidazole(π) interaction and thus the strength of the N-Fe bonds. The environment of the His ligands may also come into play in the control of the electronic properties of the coordinating imidazoles. A change in protonation and/or H-bonding state of an imidazole ligand could also alter its donor/acceptor properties to an Fe^{3+} ion,[51,52] and therefore affect the N-Fe bonds and the associated RR frequencies.

Table 1. Observed frequencies of the RR bands of K_2IrCl_6-oxidized *D. baarsii* SOR WT and its N117A, I118D, I118S, I118A and E114A mutants, excited at 647.1 nm.

RR band	WT[a]	N117A[a]	I118D[b]	I118S[b]	I118A[b]	E114A[c]	Slope RR frequency *vs* CT[d,e]	Assignment
	218	218	220	219	218	214	NS	ν_s(FeN(His))+ ν(FeS(Cys))
	241	235	240	241	240	238	-6.8 ± 2.5	ν_{as}(FeN(His))+ ν(FeS(Cys))+(FeO(Glu))
A	277	276	279	279	280	281	NS	
B	287	285	288	289	287	288	-3.7 ± 1.8	
C	299	293	302	302	302	293	-16.0 ± 1.5	ν(FeS(Cys)+ δ(Cys)
D	306	298	308	308	309	299	-18.7 ± 1.6	ν(FeS(Cys))+ δ(Cys)
E	317	311	316	314	318	313	-8.6 ± 1.9	$\delta(SC_\beta C_\alpha)$+ ν(FeS(Cys))
F	324	317	324	325	325	324	-9.7 ± 2.5	
G	344	340	345	349	346	346	-7.8 ± 3.3	$\delta(SC_\beta C_\alpha)$+$\nu$(FeS(Cys))
H	358	356	356	359	356	356	NS	$\delta(SC_\beta C_\alpha$(CO)N(CO))
I	381	380	380	380	377	376	NS	
J	396	396	396	396	395	390	NS	
K	402	401	403	404	406	402	-4.3 ± 2.4	$\delta(C_\beta C_\alpha$(CO)N(CO)) +$\delta(SC_\beta C_\alpha)$+$\nu$(FeS(Cys))
L	435	437	438	439	440	438	NS	$\delta(C_\beta C_\alpha$(CO)N(CO))
M	456	456	454	457	454	455	NS	
N	464	462	465	463	463	464	NS	
	649	648	648	650	647	648	NS	δ(His)
	658	657	658	659	658	658	-1.2 ± 0.8	$\nu(C_\alpha N)$
	713	712	712	714	713		NS	
	742	739	743	744	744	739	-7.4 ± 1.6	$\nu(SC_\beta$(Cys)) +δ(Cys)
		747				755		
	765	762	763	764	764	759	-5.4 ± 2.9	

[a] From Fig. 3A.

[b] From reference [38].

[c] From reference [41]. The RR spectrum was recorded at pH 8.50. Taking into account that the p*Ka* value for the alkaline transition for this mutant is 8.8 and that the excitation laser at 647 nm is much more closer to the CT maximum of the Fe^{3+}-Glu form (632 nm) than that of the Fe^{3+}-OH form (547 nm), this spectrum mainly originated from the Fe^{3+}-Glu form.

[d] Slopes of the linear lines in Fig. 4 are expressed in term of RR frequency shifts (cm^{-1}) for a CT band variation of 1000 cm^{-1}.

[e] NS indicates no significant value for the slope.

Trans influence of the S(Cys) ligand

As mentioned before, the ferric iron site of SOR is hexacoordinated, with the side chain of Glu47 occupying the sixth coordination position. Consequently, change in the electronegative character of the S(Cys) ligand by second coordination sphere residues, as highlighted above with the N117A mutant and other SOR *Db* derivatives,[38,41] is expected to influence through a *trans* electronic effect the Fe-O(Glu47) bond strength.[24,43] On note, this Fe-O^-(Glu47) bond strength should be reflected by the apparent pK_a of the Fe^{3+}-O(Glu47)+ $^-$OH $\rightarrow$ Fe^{3+}-OH + Glu47 alkaline transition (Fig. S1). In fact, although this apparent pK_a value represents a complex term, including a conformational reorganization and a change in geometry of the Fe^{3+} site, it remains mainly associated with the binding of the carboxylate group of Glu47 to the Fe^{3+} ion in competition with the hydroxide anion. Figure 5 shows that for the *Db* SOR derivatives, except the I118S mutant, the apparent pK_a value of the alkaline transition is related to the maximum of the CT band (Fig. 5A) and to the frequencies of RR bands involving major ν(Fe-S) stretches (Fig. 5B). It shld be noted that for the I118S mutant, the high pH conditions used to determine its apparent p*Ka* value were close to the limit of the SOR alkaline stability.[38] Consequently, the apparent p*Ka* value for the I118S mutant could be less reliable than those reported for the other SOR forms, determined in less alkaline conditions.[38] Thus, the correlations shown in Figure 5 are in line with an apparent decrease of the O(Glu47) affinity for the Fe^{3+} ion when the partial negative charge of the S(Cys) ligand is increased (CT bands in Fig. 5A) and the S-Fe bond strength is decreased (ν(Fe-S) in Fig. 5B).

These results support the validity of our CT and RR analysis and are in full agreement with a weaker S-Fe bond strength in the N117A mutant when compared to the WT SOR.

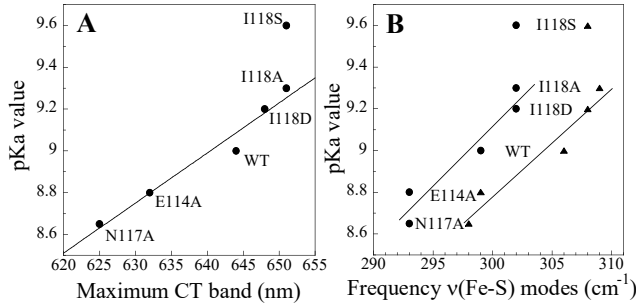

Fig. 5. Plots of the apparent pK_a for the Fe^{3+}-O^-(Glu) → Fe^{3+}-OH^- alkaline transition of *D. baarsii* WT and mutants SORs as a function in (A) of the maximum of the (Cys)S^- → Fe^{3+} charge-transfer (CT) band (●), in (B) of the frequencies of RR bands C (●) and D (▲) involving major ν(Fe-S) stretches (Table 1). The solid lines correspond to a linear correlation between the different SOR forms, without taking into account the values for the I118S mutant.

4. Discussion

The Cys ligand of the SOR iron active site has been proposed to play a central role in catalysis.[53] As described for other metalloproteins involving sulfur ligand(s), the properties of the S-Fe bond in SOR are expected to be finely tuned by second coordination sphere residues. Accordingly, in *Db* and other SORs, the Ile118 and His119 residues of the Cys116-Asn117-Ile118-His119 tetrapeptide potentially establish H-bonds through their peptide NH groups with the S(Cys116) ligand (Fig. 1 and 6) and it was demonstrated that alteration of one of these H-bonds increases the strength of the S-Fe bond.[38] The Asn117 residue, highly conserved among SOR sequences, exhibits the closest lateral chain to the sulfur atom, suggesting that it might be also involved in the control of the S-Fe bond strength.[12–18] However, in *Db* and others SORs, the X-ray structures do not show any interactions between Asn117 and the Cys ligand, the Asn117 peptide NH group as well as its lateral NH_2 group being not correctly oriented to be involved in H-bonds with the sulfur ligand (Fig. 1 and 6).[12–18]

In this work, in order to investigate a potential involvement of Asn117 toward the properties of the active site, a RR study on a N117A mutant was carried out using an excitation in the (Cys)S^- → Fe^{3+} CT band, allowing enhancements of the modes involving the Fe-S(Cys) bonds. In SORs, differences in Fe-S bond strength and in Fe-S-C_β-C_α dihedral angles govern the extent of mixing of the ν(Fe-S) and δ(Fe-S-C_β-C_α) modes as well as the complexity of the RR spectra in terms of both band frequency and band intensity.[39,40] Considering that each RR mode acts as a global or local reporter of the Fe-Cys bonding or non-bonding interactions, RR spectroscopy is potentially able to identify the effects of various mutations around the catalytic site, assuming that an attribution for the different vibrational modes has been established. Here, a RR spectra analysis has been developed to characterize in details the effects of the mutation toward the geometry and bond strengths of the $N_4S_1Fe^{3+}$ active site. By investigating the correlations between the (Cys)S^- → Fe^{3+} CT band maximum of different SOR forms with the frequency of each RR band, we assessed the contribution of the ν(S-Fe) vibration among the different RR bands.

The relevance of our analysis is fully supported by the fact that the RR band that has been experimentally identified to have the maximum contribution from a ν(S-Fe) stretch was found to exhibit one of the highest correlation with the corresponding CT band maximum (Band C, Fig. 4). In addition, the linear relation found in Figure 5 between the apparent pK_a of the alkaline transition and the CT bands and the RR frequency of the major ν(Fe-S) stretches also support the validity of this analysis. Here, our approach has been particularly useful to propose an assignment for bands for which no ^{34}S, ^{15}N and ^{54}Fe isotopic effects were reported,[39,40] and which nevertheless are notably affected by the N117A mutation.

Our data show that substitution of the Asn117 -CH_2CONH_2 side chain by the small and non-polar -CH_3 group of an alanine provokes large changes in CT position (Fig. 2A) as well as in RR modes involving the Fe-S-C_β-C_α(Cys) and Fe-N(His) bonds (Fig. 3). In fact, the 19 nm blue-shift of the CT band, the 6-8 cm^{-1} downshifts of the bands involving major ν(Fe-S) and the 3 cm^{-1} downshifts of the modes involving major ν(S-C_β) are markers of an important decrease in the Fe-S-C_β bonds strength in the mutant. This is in agreement with the increases of the Fe-O(Glu47) bond strength, as deduced from Figure 5, occurring through a *trans* axial effect of the decreased thiolate character of the S(Cys116) ligand in the N117A mutant.

Moreover, the analysis of numerous RR bands shows that the N117A mutation has also a marked effect on the conformation of the (Cys)S-Fe grouping. The intensity decrease of several bands in the mutant reflects noticeable changes in the geometry of the Fe-S-C_β-C_α bonds and conformational changes of the cysteine ligand with internal deformation of the Cys side chain (δ(S-C_β-C_α(CO)-N-C(O)). Also, the downshift of the stretching mode involving the S-C_β bond of the cysteine ligand in the mutant agrees with a decrease in strength of the S-C_α(Cys) bond and changes in the (Fe-S-C_β)-(S-C_β-C_α) dihedral angle. Finally, the significant 6 cm^{-1} downshift of a ν_{as}(Fe-N(His)) mode in the N117A mutant mostly indicates a repositioning the imidazole ring of His119 with respect to the iron.

All these spectral changes in the N117A mutant support an increase in H-bonding interactions between the Ile118 and/or His119 NH peptide group(s) and the sulfur ligand of Cys116. This conclusion is in line with previous DFT calculations on SORs models, which showed a progressive lengthening of the Fe-S distance upon a gradual increase in the H-bonding state of the S(Cys) ligand.[38]

The X-ray structures of the WT *Db* SOR suggest that Asn117 establishes three H-bonds interactions with the non-conserved Lys74 and Tyr76 residues (Fig. 6).[14,15] Two of these H-bonds could originate from the Asn117 lateral chain CO and NH_2 groups and one from its NH peptide group. The fact that Asn117 is potentially involved in three H-bonds suggests an important role in the stability of the Cys116-Asn117-Ile118-His119 tetrapeptide, with a marked impact on the rigidity of the Cys116-Asn117-Ile118 peptide skeleton. An increased of flexibility is expected in the N117A mutant, where by replacing the -CH_2CONH_2 lateral chain by a methyl group results in the loss of two H-bond interactions with Lys74 and Tyr76 residues.

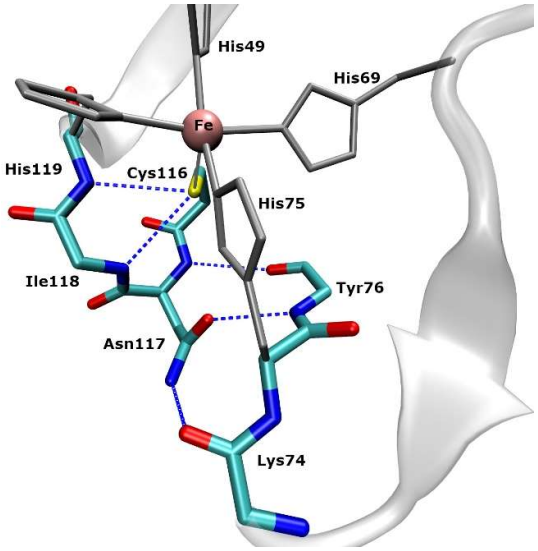

Fig. 6. Scheme of the wild-type SOR from *D. baarsii* from its crystal structure,[15] showing its iron active site (gray, thin lines) and the hydrogen bond networks (blue dashed lines) between Cys116 and Ile118 and His119 on one hand and between Asn117 and Lys74 and Tyr76 on the other hand. For clarity, side chains of Lys74, Tyr76 and Ile118 are omitted.

Thus, all the changes in frequency of the Fe-S-Cys and Fe-N(His)-involving modes in the N117A mutant are therefore consistent with a reshaping of the Cys116 side chain and the skeletal bonds of the Cys116-Asn117-Ile118-His119 tetrapeptide, bringing closer the NH groups of Ile118 and/or His119 with the S(Cys116) ligand. This conformational change in the mutant leads to a strengthening of the H-bonds between the Ile118 and/or His119 NH peptide groups and the sulfur ligand and then consequently a weakening of the S-Fe bond.

On note, one cannot also exclude the influence of a tightening effect of the H-bonds between Asn117 and Lys74 and Tyr76 on the position of the His75 and its interaction with the iron.

In conclusion, we propose that in *Db* SOR, the Asn117 residue plays a structural role with a prominent impact on the properties of the active site. Thanks to the three H-bonds interactions with residues Lys74 and Tyr76, Asn117 allows rigidifying the skeleton of the Cys116-Asn117-Ile118-His119 tetrapeptide. This results in a tight control of the H-bond distance between the Ile118 and/or His119 NH peptide and the Cys sulfur ligand, enabling a fine-tuning of the strength of the S-Fe bond. This work illustrates the roles of second coordinating sphere residues to modulate the ligand to metal bond properties in the active site of metalloenzymes.

The structural alterations by the N117A mutation characterized by the present spectroscopic investigations could have a strong effect on the SOR reactivity and in particular on the control of the evolution of the Fe^{3+}-OOH reaction intermediate. It could favor a O-O bond cleavage of the Fe^{3+}-OOH intermediate and formation of a high-valent iron-oxo species,[34] which normally does not occur in WT SOR (manuscript in preparation).

Conflicts of interest

There are no conflicts to declare.

Acknowledgements

The authors acknowledge the Labex ARCANE and CBH-EUR-GS (ANR-17-EURE-0003) for a partial financial support via the CNRS, CEA and the University of Grenoble-Alpes.

Notes and references

1 J. A. Imlay, *Nat. Rev. Microbiol.*, 2013, **11**, 443–454.
2 C. C. Winterbourn, *Nat. Chem. Biol.*, 2008, **4**, 278–286.
3 J. A. Imlay, *Annu. Rev. Biochem.*, 2008, **77**, 755–776.
4 F. E. Jenney, M. F. Verhagen, X. Cui and M. W. Adams, *Science*, 1999, **286**, 306–309.
5 M. Lombard, M. Fontecave, D. Touati and V. Nivière, *J. Biol. Chem.*, 2000, **275**, 115–121.
6 D. M. Kurtz, *Acc. Chem. Res.*, 2004, **37**, 902–908.
7 V. Nivière and M. Fontecave, *J. Biol. Inorg. Chem. JBIC Publ. Soc. Biol. Inorg. Chem.*, 2004, **9**, 119–123.
8 A. S. Pereira, P. Tavares, F. Folgosa, R. M. Almeida, I. Moura and J. J. G. Moura, *Eur. J. Inorg. Chem.*, 2007, **2007**, 2569–2581.
9 M. C. Martins, C. V. Romão, F. Folgosa, P. T. Borges, C. Frazão and M. Teixeira, *Free Radic. Biol. Med.*, 2019, **140**, 36–60.
10 F. Auchère, S. R. Pauleta, P. Tavares, I. Moura and J. J. G. Moura, *J. Biol. Inorg. Chem. JBIC Publ. Soc. Biol. Inorg. Chem.*, 2006, **11**, 433–444.
11 J. P. Emerson, E. D. Coulter, R. S. Phillips and D. M. Kurtz, *J. Biol. Chem.*, 2003, **278**, 39662–39668.
12 A. V. Coelho, P. Matias, V. Fülöp, A. Thompson, A. Gonzalez and M. A. Carrondo, *JBIC J. Biol. Inorg. Chem.*, 1997, **2**, 680–689.
13 A. P. Yeh, Y. Hu, F. E. Jenney, M. W. Adams and D. C. Rees, *Biochemistry*, 2000, **39**, 2499–2508.
14 V. Adam, A. Royant, V. Nivière, F. P. Molina-Heredia and D. Bourgeois, *Struct. Lond. Engl. 1993*, 2004, **12**, 1729–1740.
15 G. Katona, P. Carpentier, V. Nivière, P. Amara, V. Adam, J. Ohana, N. Tsanov and D. Bourgeois, *Science*, 2007, **316**, 449–453.
16 T. Santos-Silva, J. Trincão, A. L. Carvalho, C. Bonifácio, F. Auchère, P. Raleiras, I. Moura, J. J. G. Moura and M. J. Romão, *J. Biol. Inorg. Chem. JBIC Publ. Soc. Biol. Inorg. Chem.*, 2006, **11**, 548–558.
17 C. M. Sousa, P. Carpentier, P. M. Matias, F. Testa, F. Pinho, P. Sarti, A. Giuffrè, T. M. Bandeiras and C. V. Romão, *Acta Crystallogr. D Biol. Crystallogr.*, 2015, **71**, 2236–2247.
18 C. V. Romão, P. M. Matias, C. M. Sousa, F. G. Pinho, A. F. Pinto, M. Teixeira and T. M. Bandeiras, *Biochemistry*, 2018, **57**, 5271–5281.
19 C. Lucchetti-Miganeh, D. Goudenège, D. Thybert, G. Salbert and F. Barloy-Hubler, *BMC Microbiol.*, 2011, **11**, 105.
20 M. Archer, R. Huber, P. Tavares, I. Moura, J. J. Moura, M. A. Carrondo, L. C. Sieker, J. LeGall and M. J. Romão, *J. Mol. Biol.*, 1995, **251**, 690–702.
21 F. Bonnot, S. Duval, M. Lombard, J. Valton, C. Houée-Levin and V. Nivière, *J. Biol. Inorg. Chem. JBIC Publ. Soc. Biol. Inorg. Chem.*, 2011, **16**, 889–898.
22 F. Folgosa, C. M. Cordas, J. A. Santos, A. S. Pereira, J. J. G. Moura, P. Tavares and I. Moura, *Biochem. J.*, 2011, **438**, 485–494.

23 M. Horch, T. Utesch, P. Hildebrandt, M. A. Mroginski and I. Zebger, *Phys. Chem. Chem. Phys. PCCP*, 2016, **18**, 23053–23066.
24 V. Nivière, M. Asso, C. O. Weill, M. Lombard, B. Guigliarelli, V. Favaudon and C. Houée-Levin, *Biochemistry*, 2004, **43**, 808–818.
25 J. P. Emerson, E. D. Coulter, D. E. Cabelli, R. S. Phillips and D. M. Kurtz, *Biochemistry*, 2002, **41**, 4348–4357.
26 J. V. Rodrigues, I. A. Abreu, D. Cabelli and M. Teixeira, *Biochemistry*, 2006, **45**, 9266–9278.
27 F. Bonnot, T. Molle, S. Ménage, Y. Moreau, S. Duval, V. Favaudon, C. Houée-Levin and V. Nivière, *J. Am. Chem. Soc.*, 2012, **134**, 5120–5130.
28 A. Dey, F. E. Jenney, M. W. W. Adams, M. K. Johnson, K. O. Hodgson, B. Hedman and E. I. Solomon, *J. Am. Chem. Soc.*, 2007, **129**, 12418–12431.
29 P. H.-L. Sit, A. Migliore, M.-H. Ho and M. L. Klein, *J. Chem. Theory Comput.*, 2010, **6**, 2896–2909.
30 R. David, H. Jamet, V. Nivière, Y. Moreau and A. Milet, *J. Chem. Theory Comput.*, 2017, **13**, 2987–3004.
31 C. Mathé, T. A. Mattioli, O. Horner, M. Lombard, J.-M. Latour, M. Fontecave and V. Nivière, *J. Am. Chem. Soc.*, 2002, **124**, 4966–4967.
32 C. Mathé, V. Nivière, C. Houée-Levin and T. A. Mattioli, *Biophys. Chem.*, 2006, **119**, 38–48.
33 O. Horner, J.-M. Mouesca, J.-L. Oddou, C. Jeandey, V. Nivière, T. A. Mattioli, C. Mathé, M. Fontecave, P. Maldivi, P. Bonville, J. A. Halfen and J.-M. Latour, *Biochemistry*, 2004, **43**, 8815–8825.
34 F. Bonnot, E. Tremey, D. von Stetten, S. Rat, S. Duval, P. Carpentier, M. Clemancey, A. Desbois and V. Nivière, *Angew. Chem. Int. Ed Engl.*, 2014, **53**, 5926–5930.
35 S. Shaik, S. Cohen, Y. Wang, H. Chen, D. Kumar and W. Thiel, *Chem. Rev.*, 2010, **110**, 949–1017.
36 M. D. Clay, F. E. Jenney, P. L. Hagedoorn, G. N. George, M. W. W. Adams and M. K. Johnson, *J. Am. Chem. Soc.*, 2002, **124**, 788–805.
37 C. Berthomieu, F. Dupeyrat, M. Fontecave, A. Verméglio and V. Nivière, *Biochemistry*, 2002, **41**, 10360–10368.
38 E. Tremey, F. Bonnot, Y. Moreau, C. Berthomieu, A. Desbois, V. Favaudon, G. Blondin, C. Houée-Levin and V. Nivière, *J. Biol. Inorg. Chem. JBIC Publ. Soc. Biol. Inorg. Chem.*, 2013, **18**, 815–830.
39 M. D. Clay, F. E. Jenney, H. J. Noh, P. L. Hagedoorn, M. W. W. Adams and M. K. Johnson, *Biochemistry*, 2002, **41**, 9833–9841.
40 M. D. Clay, J. P. Emerson, E. D. Coulter, D. M. Kurtz and M. K. Johnson, *J. Biol. Inorg. Chem. JBIC Publ. Soc. Biol. Inorg. Chem.*, 2003, **8**, 671–682.
41 C. Mathé, C. O. Weill, T. A. Mattioli, C. Berthomieu, C. Houée-Levin, E. Tremey and V. Nivière, *J. Biol. Chem.*, 2007, **282**, 22207–22216.
42 T. Picaud, C. Le Moigne, B. Loock, M. Momenteau and A. Desbois, *J. Am. Chem. Soc.*, 2003, **125**, 11616–11625.
43 C. Mathé, V. Nivière and T. A. Mattioli, *J. Am. Chem. Soc.*, 2005, **127**, 16436–16441.
44 R. S. Czernuszewicz, L. K. Kilpatrick, S. A. Koch and T. G. Spiro, *J. Am. Chem. Soc.*, 1994, **116**, 7134–7141.
45 S. Han, R. S. Czernuszewicz and T. G. Spiro, *J. Am. Chem. Soc.*, 1989, **111**, 3496–3504.
46 D. Qiu, L. Kilpatrick, N. Kitajima and T. G. Spiro, *J. Am. Chem. Soc.*, 1994, **116**, 2585–2590.
47 D. F. Blair, G. W. Campbell, W. K. Cho, A. M. English, H. A. Fry, V. Lum, K. A. Norton, J. R. Schoonover and S. I. Chan, *J. Am. Chem. Soc.*, 1985, **107**, 5755–5766.
48 S. Todorovic, J. V. Rodrigues, A. F. Pinto, C. Thomsen, P. Hildebrandt, M. Teixeira and D. H. Murgida, *Phys. Chem. Chem. Phys. PCCP*, 2009, **11**, 1809–1815.
49 A. F. Pinto, C. V. Romão, L. C. Pinto, H. Huber, L. M. Saraiva, S. Todorovic, D. Cabelli and M. Teixeira, *J. Biol. Inorg. Chem. JBIC Publ. Soc. Biol. Inorg. Chem.*, 2015, **20**, 155–164.
50 P. Tavares, N. Ravi, J. J. Moura, J. LeGall, Y. H. Huang, B. R. Crouse, M. K. Johnson, B. H. Huynh and I. Moura, *J. Biol. Chem.*, 1994, **269**, 10504–10510.
51 R. J. Sundberg and R. B. Martin, *Chem. Rev.*, 1974, **74**, 471–517.
52 A. Desbois and M. Lutz, *Eur. Biophys. J.*, 1992, **20**, 321–335.
53 J. A. Kovacs, *Chem. Rev.*, 2004, **104**, 825–848.